

Muon tagging using a Match- χ^2 based Soft Muon Tagger in top quark analyses using data from the ATLAS detector

Jacobo Ezequiel Blanco

Department of Physics
Royal Holloway, University of London



A thesis submitted to the University of London for the
Degree of Doctor of Philosophy

March 24, 2014

DECLARATION

I confirm that the work presented in this thesis is my own. Where information has been derived from other sources, I confirm that this has been indicated in the document.

Jacobo Ezequiel Blanco

Abstract

This is an abstract

Contents

| | | |
|----------|---|-----------|
| 1 | Introduction and motivation | 7 |
| 2 | The Standard Model of Particle Physics | 8 |
| 2.1 | Quantum Electrodynamics | 9 |
| 2.2 | Quantum Chromodynamics | 11 |
| 2.3 | Weak Interactions | 12 |
| 2.3.1 | Electroweak Unification and the Higgs mechanism | 15 |
| 3 | Top-quark physics | 16 |
| 3.1 | Top quark production | 16 |
| 3.2 | Top quark decay modes | 16 |
| 4 | The LHC and the ATLAS Detector | 17 |
| 4.1 | The Large Hadron Collider | 17 |
| 4.2 | The ATLAS detector | 17 |
| 5 | Identifying b-jet, and the Match χ^2 based Soft Muon Tagger | 18 |
| 5.1 | b -jet tagging methodology | 18 |
| 5.2 | The Match- χ^2 Soft Muon Tagger | 18 |
| 6 | Calibration of the Soft Muon Tagger for 2012 ATLAS Data | 19 |
| 6.1 | Tag and probe selection | 19 |
| 6.2 | Vertexing | 19 |
| 6.3 | Invariant mass fitting | 19 |
| 6.4 | Efficiencies | 19 |

| | | |
|----------|--|-----------|
| 7 | Measurement of the $t\bar{t}$ cross-section in the single-lepton channel using SMT | 20 |
| 7.1 | Data and Monte Carlo samples | 20 |
| 7.2 | Object selection and event selection | 20 |
| 7.3 | Re-weighting of the b-quark to muon transition BR | 20 |
| 7.4 | Data-driven background selection | 20 |
| 7.5 | Systematics uncertainties | 20 |
| 7.6 | Results and conclusion | 20 |
| 8 | Muon Tagging in a boosted $t\bar{t}$ environment | 21 |
| 8.1 | Examination of the topology of a boosted event | 22 |
| 8.2 | Samples and muon selection | 24 |
| 8.2.1 | Muon selection | 24 |
| 8.3 | Efficiency definition | 25 |
| 8.4 | Results | 30 |
| 8.4.1 | Background | 30 |
| 9 | Conclusions | 34 |

List of Figures

| | | |
|-----|--|----|
| 2.1 | The interaction vertex described by QED. One can obtain all possible vertex shapes by rotating this basic vertex and assigning the appropriate electric charge and making sure to conserve lepton flavour across the vertex. | 11 |
| 2.2 | Feynman diagrams of the process $e^+e^- \rightarrow e^+e^-$ allowed in QED. Note that these are the simplest diagrams, also known as tree level diagrams, and additional vertexes can be added to produce higher-order diagrams of the same process. | 11 |
| 2.3 | Diagrams of the fundamental interaction vertices described by quantum chromodynamics. | 12 |
| 2.4 | The neutral current and charged current vertexes allowed via the Weak force. Where f can be an e , μ or τ and ν_ℓ is the corresponding lepton neutrino of the same flavour. One can obtain all possible vertex shapes by rotating these basic vertexes and assigning the appropriate electric charge and making sure to conserve lepton flavour across the vertex. | 13 |
| 2.5 | Neutral current weak scattering vertex | 13 |
| 8.1 | Diagram of the semileptonic $t\bar{t}$ decay | 22 |
| 8.2 | Simple diagrams representing the possible configurations in boosted and non-boosted events | 23 |
| 8.3 | The angular separation (ΔR) between the truth W muon and the corresponding b -quark in boosted top quark events. The data corresponds to a Z' with a mass of 1.6 TeV. | 23 |

| | | |
|-----|---|----|
| 8.4 | The truth transverse momentum of the top/anti-top quarks in the event. This distribution corresponds to a Z' with a mass of 1.6 TeV. Note the peak at approximately half of the Z' mass. | 23 |
| 8.5 | Control plots for muons which pass the χ^2_{match} tagger selection for all tested Z' mass points. | 26 |
| 8.6 | Control plots for muons which pass the mini-isolation selection for all tested Z' mass points. | 27 |
| 8.7 | Structure of the efficiency measurement. | 28 |
| 8.8 | Efficiency of mini-isolation ($k_T = 10$) and χ^2_{match} muon tagger as a function of the angular separation between the reconstructed muon and the nearest reconstructed jet. Note the dip in the mini-isolation efficiency at low ΔR . In the nominal analysis an overlap removal between the jet and the muon is applied. | 31 |
| 8.9 | Efficiency of mini-isolation ($k_T = 10$) and χ^2_{match} muon tagger as a function of the transverse momentum of the muon. | 32 |

List of Tables

| | | |
|-----|---|----|
| 2.1 | A summary of all elementary particles described by The Standard Model. Note the various groupings and divisions including by spin, generation and particle type. Within the fermion sector the quarks are shown in yellow and the leptons are shown in green. These are grouped into three different generations traditionally denoted by roman numerals. The force mediators known as gauge bosons are shown in blue and finally the recently discovered Higgs boson with a spin of zero. | 10 |
| 2.2 | A summary of the four fundamental forces ordered by relative strength. These are approximated relative strengths for the purpose of demonstrating the hierarchy of forces as a function of their strength. A more accurate determination of the interaction strength depends on the details of the interaction itself. Note however the order-of-magnitude differences in the relative strengths of these forces. Note that the graviton is the theoretical boson responsible for mediating gravitational interactions, it is not part of the SM. | 10 |
| 8.1 | Summary of the samples used in this b | 24 |
| 8.2 | Muon reconstruction selection used by Mini-Isolation and by Muon Tagging | 25 |
| 8.3 | The efficiency measured in a selected background events. | 33 |

Chapter 1

Introduction and motivation

This part will include an overview summary of the body of work presented in the thesis including a scientific motivation for the use of the soft muon tagger as a method for b-jet tagging and muon tagging.

Chapter 2

The Standard Model of Particle Physics

Particle physics is the study of the most fundamental constituents of matter and their interactions. The best current description of these interactions is known as The Standard Model of Particle Physics (SM); a group of theories that cover all currently known particles and their interactions. The SM was developed through-out the latter half of the 20th century and has seen tremendous success in predicting the behaviour of our universe at the most fundamental level. The SM has stood the test of time and rigorous examination by numerous experiments. The last piece to be confirmed was the existence of the Higgs boson, which in turn points to the existence of the so-called Higgs field. Evidence of the elusive Higgs were observed by the ATLAS and CMS experiments at CERN in the latter half of 2013.

The SM describes the nature of the interactions of the fundamental constituents of our universe in terms of the three different fundamental forces: Strong, Weak and Electromagnetic each described by a specific theory. Note that the most familiar of the forces, gravity, is not included in this list. The Standard Model does not incorporate a description of gravity, however the development of such description is the subject of much interest for those creating theories that go Beyond the Standard Model (BSM).

The Standard Model classifies particles into several categories depending on their properties and allowed interactions. Particles which have a half-integer spins (e.g. $\frac{1}{2}$,

$\frac{3}{2}, \dots$) are known as Fermions, and particles with integer spins (e.g. 0, 1, ...) are known as Bosons. A summary of all elementary particles described by The Standard Model can be found in Table 2.1.

Fermions can be divided into two subgroups: Quarks, which can interact by the strong, weak and electromagnetic forces and leptons which can only interact by the weak and electromagnetic forces. Each group contains six particles which are categorized into 3 distinct generations. For every matter fermion (f) there is an equivalent antimatter partner (\bar{f}) which possesses the same characteristics as its matter companion but is opposite in electrical charge. Thus 12 matter particles are combined with 12 antimatter partners for a total of 24 elementary particles which form all material in the universe.

The interaction between fermions are occur via the exchange of spin one particles known as bosons. Each force is mediated by one or more bosons (Table 2.2). The strong force is mediated by a set of massless bosons known as the gluons. The weak force is mediated by a neutral massive boson known as the Z boson and a pair of charged massive bosons known as the W bosons. Finally, the electromagnetic force is mediated by a massless boson known as the photon. From Note that each boson has an antimatter partner however some are indistinguishable from their matter partner. A summary of their properties is show in Table 2.1.

2.1 Quantum Electrodynamics

The interaction of particles via the electromagnetic force is described by Quantum Electrodynamics or QED. These interactions are mediated by the massless neutral boson known as the photon and the strength of the interaction is characterized by the fine-structure constant α . All electrically charged fermions are allowed to interact, however since the photon itself is not charged, no self-interaction is allowed within QED. One of the simplest examples of QED interactions is the decay of a photon into a fermion/antifermion pair (Figure 2.1). Note that the electric charge is conserved across the vertex, so for example $\gamma \rightarrow e^+e^+$ is not allowed within QED.

By combining different forms of this vertex one can build every possible QED interaction. Electron-Positron pairs can annihilate to create energy in the form of a photon

Table 2.1: A summary of all elementary particles described by The Standard Model. Note the various groupings and divisions including by spin, generation and particle type. Within the fermion sector the quarks are shown in yellow and the leptons are shown in green. These are grouped into three different generations traditionally denoted by roman numerals. The force mediators known as gauge bosons are shown in blue and finally the recently discovered Higgs boson with a spin of zero.

| | | Fermions ($s = \frac{1}{2}$) | | | Bosons ($s = 0$) | Higgs ($s = 1$) |
|---------|--|---|---|---|---|--|
| | | I | II | III | | |
| Quarks | | $+\frac{2}{3}$ 2.3 MeV <i>u</i> Up | $+\frac{2}{3}$ 1.275 GeV <i>c</i> Charm | $+\frac{2}{3}$ 173.07 GeV <i>t</i> Top | 0 0 MeV γ Photon (EM) | 0 126.07 GeV H^0 Higgs boson |
| | | $-\frac{1}{3}$ 4.8 MeV <i>d</i> Down | $-\frac{1}{3}$ 95 MeV <i>s</i> Strange | $-\frac{1}{3}$ 4.18 GeV <i>b</i> Bottom | ± 1 80.4 GeV W^\pm W boson (Weak) | |
| Leptons | | -1 0.511 MeV <i>e</i> Electron | -1 105.7 MeV μ Muon | -1 1.777 GeV τ Tau | 0 91.2 GeV <i>Z</i> Z boson (Weak) | |
| | | 0 < 2.2 eV ν_e Electron Neutrino | 0 < 0.17 MeV ν_μ Muon Neutrino | 0 15.5 MeV ν_τ Tau Neutrino | 0 0 MeV <i>g</i> Gluon (Strong) | q mass symbol name (force) |

Table 2.2: A summary of the four fundamental forces ordered by relative strength. These are approximated relative strengths for the purpose of demonstrating the hierarchy of forces as a function of their strength. A more accurate determination of the interaction strength depends on the details of the interaction itself. Note however the order-of-magnitude differences in the relative strengths of these forces. Note that the graviton is the theoretical boson responsible for mediating gravitational interactions, it is not part of the SM.

| Name | Relative Strength | Boson |
|-----------------|-------------------|-------------------|
| Strong | 10^{38} | Gluons |
| Electromagnetic | 10^{36} | Photon |
| Weak | 10^{25} | W^\pm and Z^0 |
| Gravity | 1 | Graviton* |

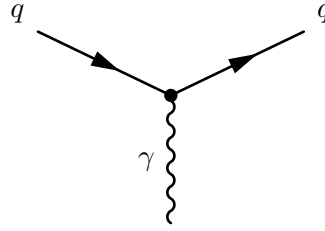
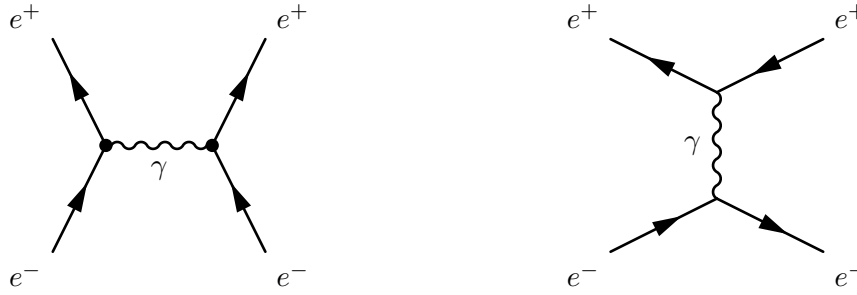


Figure 2.1: The interaction vertex described by QED. One can obtain all possible vertex shapes by rotating this basic vertex and assigning the appropriate electric charge and making sure to conserve lepton flavour across the vertex.



(a) Electron-Positron pair annihilation mediated by a photon.

(b) Electron-Positron pair scattering via the emission of a photon.

Figure 2.2: Feynman diagrams of the process $e^+e^- \rightarrow e^+e^-$ allowed in QED. Note that these are the simplest diagrams, also known as tree level diagrams, and additional vertexes can be added to produce higher-order diagrams of the same process.

(Figure 2.2a) and then subsequently decay into an additional Electron-Positron pair. Electrons can scatter by emitting a photon which is then absorbed by a positron (Figure 2.2b) this process is known as Bhabha scattering.

2.2 Quantum Chromodynamics

Interactions via the strong force are described in the theory of Quantum Chromodynamics or QCD. These interactions are mediated by a set of massless neutral bosons known as gluons. QCD introduces the concept of "colour", which similarly to electrical charge, determines the possible interactions that can occur via the strong force. "Colour" can take three states red (antired), blue (antiblue), green (antigreen). Both quarks and gluons possess colour and as a result gluons, unlike photons, can self-interact (Figure 2.3)). As with electrical charge, colour-charge must also be conserved. Thus in the scattering process $q \rightarrow q + g$ shown in Figure 2.3a the flavour of the quark may not change but

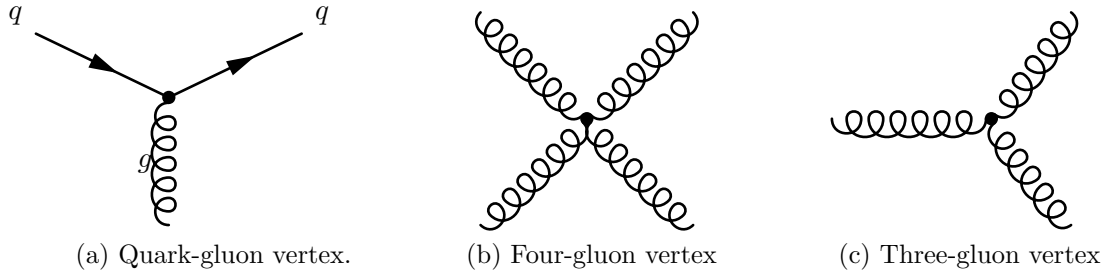


Figure 2.3: Diagrams of the fundamental interaction vertices described by quantum chromodynamics.

the colour-charge does and the gluon carries away the difference in colour. There are eight different gluons that can participate in QCD interactions each with a different colour-charge combination. Note that there is a ninth combination ($R\bar{R} + G\bar{G} + B\bar{B}$) which is overall colorless so it cannot take part in interactions.

In an analogous fashion to screening which occurs with electric charges, quark-antiquark pairs act like dipoles which screen the true colour charge of the central quark. However since gluons also carry colour, they have the opposite effect of anti-screening which amplify and change the observed colour of the quark. Which effects wins out depends on the number of colours in the theory and the number of quark flavours. As it is with three colour states and six different quark flavours, anti-screening is the overall dominant effect. As a result the colour potential decreases with distance and quarks experience very little potential when very near to each other. This effect is known as asymptotic freedom and results in quarks only existing within colorless bound states known as hadrons.

Hadrons can be divided into two categories: Mesons, which contain a quark and an antiquark ($q\bar{q}$); and Baryons which are made of three quarks (or antiquarks) each with a different (anti)colour-charge to result in a colourless composite particle. Common examples of baryons are protons (uud) and neutrons (udd) which are the building blocks of atomic nuclei.

2.3 Weak Interactions

The final type of interaction involves the so-called weak force. The weak force is responsible for β^- decay ($n \rightarrow p + e^- + \bar{\nu}_e$) and β^+ decay ($p \rightarrow n + e^+ + \nu_e$). Interactions via

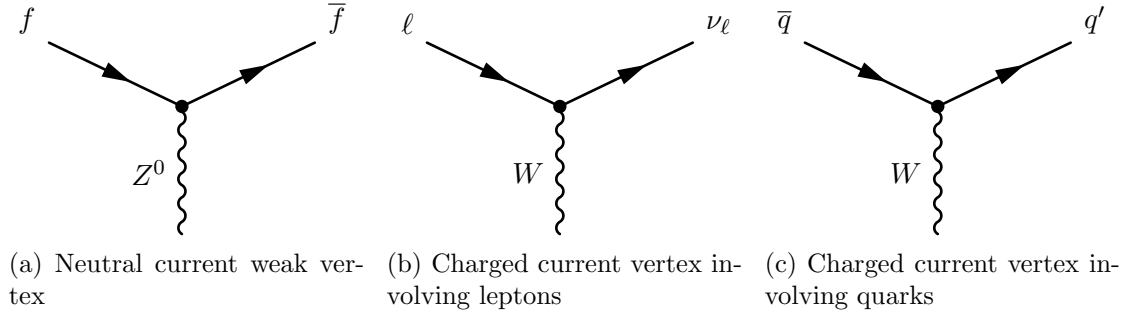


Figure 2.4: The neutral current and charged current vertexes allowed via the Weak force. Where f can be an e , μ or τ and ν_ℓ is the corresponding lepton neutrino of the same flavour. One can obtain all possible vertex shapes by rotating these basic vertexes and assigning the appropriate electric charge and making sure to conserve lepton flavour across the vertex.

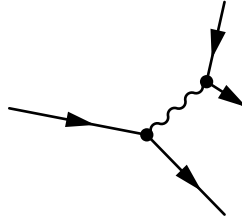


Figure 2.5: Neutral current weak scattering vertex

the Weak force are mediated by a single neutral massive boson and two charged massive bosons. Since the bosons responsible for weak interactions are massive, the range of interaction is very short, unlike electromagnetic interactions via a massless photon.

All fermions can take part in interactions via the Weak force. Interactions involving only leptons are simpler so we shall begin our review there. The Weak neutral vertex is very similar to the basic vertex seen in QED (2.1). A valid interaction via the weak force is then formed by combining these simple vertexes (Figure 2.4) while taking care to conserve electric charge and lepton flavour. An example of a leptonic weak interaction is muon decay ($\mu \rightarrow \nu_\mu W^- \rightarrow \nu_\mu e^- \bar{\nu}_e$) shown in Figure 2.5.

The Weak interactions are relatively simple and straight-forward as far as leptons are concerned. Things are not so when including quarks in weak interactions. The neutral vertex is similar to that of the leptonic version, a quark can emit a Z boson or a Z boson can decay forming a quark-antiquark pair. The charged current then changes the flavour of an up-type quark into a down-type quark (or vice-versa) with a W boson of the appropriate charge (Figure 2.4c). It is possible for a Weak interaction to change

the flavour of a quark across families. A well known example of such an interaction is Kaon decay ($K^+ \rightarrow \mu^+ \nu_\mu$). In order to account for this interaction and preserve the universality of weak interactions, Nicola Cabibbo postulated that the states that couple to the charged current are really a mixture of 'rotated' quark states:

$$\begin{pmatrix} u \\ d' \end{pmatrix} = \begin{pmatrix} c \\ s' \end{pmatrix} \quad \begin{pmatrix} t \\ b' \end{pmatrix} \quad (2.1)$$

where

$$d' = d \cos \theta_c + s \sin \theta_c \quad (2.2a)$$

$$s' = -d \sin \theta_c + s \cos \theta_c \quad (2.2b)$$

This introduces an arbitrary parameter into the theory known as the quark mixing angle or the Cabibbo angle, named after Nicola Cabibbo who developed the phenomenon of quark mixing. The introduction of quark mixing has the effect of attenuating the interaction strength at vertexes involving multiple quark generations. Interactions which cross one generation ($u \rightarrow s$) are said to be Cabibbo Suppressed while those that cross two generations ($u \rightarrow b$) are Doubly Cabibbo suppressed.

Taking into account the three quark generations, quark mixing can be expressed in matrix notation as shown in Equation 2.3. This unitary matrix is known as the Cabibbo-Kobayashi-Maskawa Matrix (CKM Matrix) after Cabibbo which initially postulated quark mixing and Makoto Kobayashi and Toshihide Maskawa who later added an additional generation, containing the top and bottom quarks, to the matrix.

$$\begin{pmatrix} d' \\ s' \\ b' \end{pmatrix} = V_{CKM} \begin{pmatrix} d \\ s \\ b \end{pmatrix} = \begin{pmatrix} V_{ud} & V_{us} & V_{ub} \\ V_{cd} & V_{cs} & V_{cb} \\ V_{td} & V_{ts} & V_{tb} \end{pmatrix} \begin{pmatrix} d \\ s \\ b \end{pmatrix} \quad (2.3)$$

The elements of the CKM matrix have been measured and the latest accepted results are summarized in 2.5. The interaction strength is then proportional to $|V_{ij}|^2$. Including all three generations the sum of all possible transitions from a given quark, q , is unity:

$$\sum |V_{qi}|^2 = 1 \quad (2.4)$$

Note that the term V_{tb} is approximately unity and by far dominates over the other V_{tj} terms. This means that the top-quark transitions almost exclusively into a b -quark ($t \rightarrow Wb$) with transitions $t \rightarrow Ws$ and $t \rightarrow Wd$ being exceedingly rare. The Soft Muon Tagger which is the focus of this thesis relies on Weak semileptonic decays of b -quarks. From 2.5 one can see that the transition $b \rightarrow c$ dominates over $b \rightarrow u$.

$$V_{CKM} = \begin{pmatrix} 0.97427 \pm 0.00015 & 0.22534 \pm 0.00065 & 0.00351^{+0.00015}_{-0.00014} \\ 0.22520 \pm 0.00065 & 0.97344 \pm 0.00016 & 0.0412^{+0.0011}_{-0.0005} \\ 0.00867^{+0.00029}_{-0.00031} & 0.0404^{+0.0011}_{-0.0005} & 0.999146^{+0.000021}_{-0.000046} \end{pmatrix} \quad (2.5)$$

An additional unique feature of Weak interactions is that the charge conjugation-parity (CP) symmetry is violated. The operator C denotes the change of a particle by its antiparticle partner and P denotes a reversal of helicity (the projection of spin onto the momentum of a particle). A clear violation of C and P was observed in the radioactive decay of Cobalt-60, where the resulting electrons were preferentially emitted in the opposite direction of the nuclear spin of the Cobalt. Thus weak currents only couple to left-handed neutrinos (or right-handed antineutrinos) this is then a violation of parity. Additionally charge symmetry is also violated since a left-handed neutrino is preferentially picked over a left-handed antineutrino. Finally in 1964 CP violation was observed in the decay of neutral kaon.

Thus the probability of $\bar{a} \rightarrow \bar{b}$ is not equal to that of $a \rightarrow b$. The existence of CP violation has interesting consequences for the formation of the early universe. The preferential production of matter over antimatter in CP violating interactions would shift the balance in favour of matter resulting in a universe similar to our own.

2.3.1 Electroweak Unification and the Higgs mechanism

Chapter 3

Top-quark physics

Since this thesis will focus mostly on top quark physics a strong emphasis is put on the description of processes involving this quark

3.1 Top quark production

3.2 Top quark decay modes

Chapter 4

The LHC and the ATLAS Detector

This section will include a description of the Large Hadron Collider and the ATLAS detector technology with particular emphasis on those aspects that allow for precision measurement of muons and top quark physics studies.

4.1 The Large Hadron Collider

4.2 The ATLAS detector

Chapter 5

Identifying b -jet, and the Match χ^2 based Soft Muon Tagger

This section will include a description of several current methodologies for b -jet tagging and a detailed description of the Match- χ^2 Soft Muon Tagger.

5.1 b -jet tagging methodology

5.2 The Match- χ^2 Soft Muon Tagger

Chapter 6

Calibration of the Soft Muon Tagger for 2012 ATLAS Data

A discussion of the calibration of the soft muon tagger for use in 2012 data. Most of the tag and probe methodology used for 2011 is repeated in 2012 with some exceptions particularly in the treatment of pile-up and certain corrections applied which are unique to 2012 data.

6.1 Tag and probe selection

6.2 Vertexing

6.3 Invariant mass fitting

6.4 Efficiencies

Chapter 7

Measurement of the $t\bar{t}$ cross-section in the single-lepton channel using SMT

This section will discuss the measurement of the $t\bar{t}$ cross-section in the single-lepton channel with an emphasis on the electron multijet background estimation conducted.

7.1 Data and Monte Carlo samples

This section will

7.2 Object selection and event selection

7.3 Re-weighting of the b-quark to muon transition BR

7.4 Data-driven background selection

7.5 Systematics uncertainties

7.6 Results and conclusion

Chapter 8

Muon Tagging in a boosted $t\bar{t}$ environment

The large center-of-mass energies at which collisions occur at the LHC allows for the production of very high mass particles. Several Beyond the SM (BSM) theories predict the existence of high mass particles which decay primarily top quark pairs. An example of hypothetical model which predict high mass $t\bar{t}$ resonances is the topcolor assisted technicolor model (TC2), which predicts the existence of a leptophobic Z' boson. The resultant top quark pair provides a well understood probe to search for such hypothetical particles.

The Z' could potentially have a mass on the order of several TeV. As a result their decay product would be produced in the detector with very large momentum. These top quarks are said to be boosted. In terms of the subsequent top decay, the resultant bottom quark and W boson are expected to emerge in a collimated cone. The events thus appear as two large back-to-back jets. If the W decays leptonically, the W lepton is expected to lie very close to or within the b -jet. If the W decays hadronically all three jets will appear to merge into a single 'fat' jet.

In this chapter the results of a feasibility study conducted to determine the viability of using the χ^2_{match} tagger to tag W muons from boosted top-quark decays is presented and discussed. Note that this is in contrast to the cross-section analysis detailed in a previous chapter where the muon tagged came from the semileptonic decay of b -quarks.

Figure 8.1: Diagram of the semileptonic $t\bar{t}$ decay

The boost is expected to be related to the mass of the Z' produced, so a higher mass Z' would decay into more collimated jets. The environment that results is thus very similar to that of a semileptonic b -decay, a muon buried inside of a b -jet.

No evidence for such a resonance has been observed and limits have been placed on the production rate of these resonance for various benchmark models. A leptophobic topcolor Z' of mass less than 1.74 TeV has been excluded using 4.7 fb^{-1} of pp collision data collected by ATLAS with a center-of-mass energy $\sqrt{s} = 7 \text{ TeV}$ [3]. Additionally a more recent analysis using 14.3 fb^{-1} of $\sqrt{s} = 8 \text{ TeV}$ data collected at ATLAS excluded a Z' with a mass less than 1.8 TeV at 95% confidence level [1]. The analysis detailed here is based on the 7 TeV analysis. Similar analyses performed with data collected by CMS have excluded Z' candidates for similar benchmark models [2, 4, 5].

The performance of SMT is compared to the current method for selecting muons known as mini-isolation. In addition a short performance study to determine the viability of using SMT to tag b -jets in boosted top events is also presented. Firstly, a short examination of the topology of a boosted event is presented.

8.1 Examination of the topology of a boosted event

In order to perform an effective feasibility study, it is important to understand the signature left by boosted events in the detector. There are certain expectations regarding the momentum distribution of the various product particles from the decay of the top as well as their angular separation. As with the cross-section analysis presented in Chapter 7, this study focuses on the semileptonic decays of top quark pairs as shown in Figure 8.1.

It is expected that events where the momentum of the top quarks is higher, exhibit stronger collimation between the W muon and the b -quark. This results in a situation very similar to that exploited for muon tagging in Section 7.

where a muon from the semileptonic decay of a b -quark is merged with the constituents of the resulting b -jet. Figure 8.2 illustrates both scenarios. As such it is

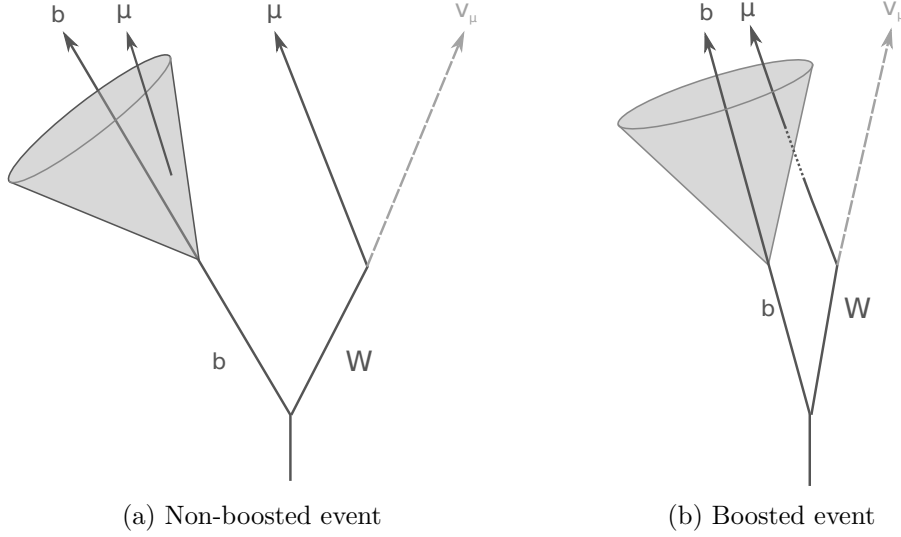


Figure 8.2: Simple diagrams representing the possible configurations in boosted and non-boosted events

Figure 8.3: The angular separation (ΔR) between the truth W muon and the corresponding b -quark in boosted top quark events. The data corresponds to a Z' with a mass of 1.6 TeV.

possible to use the soft muon tagger to tag W muons in boosted events. As SMT is designed to work in energetically "busy" sectors of the detector, it is ideally suited to probe highly boosted events with highly final-state particles.

As can be seen from Figure 8.3 the increase in boost does result in the W muon and b -quark emerging closer. Note that the fraction of events below the SMT requirement of $\Delta R(\mu, jet) < 0.5$ increases with increased top-quark p_T . Additionally Figure 8.4 shows that the top p_T distribution peaks at just below half of the mass of the Z' boson, thus the large portion of the candidate muons in the sample will pass the aforementioned separation requirement.

Figure 8.4: The truth transverse momentum of the top/anti-top quarks in the event. This distribution corresponds to a Z' with a mass of 1.6 TeV. Note the peak at approximately half of the Z' mass.

Table 8.1: Summary of the samples used in this b

| Mass (GeV) |
|------------|
| 1000 |
| 1300 |
| 1600 |
| 2000 |
| 2500 |
| 3000 |

8.2 Samples and muon selection

This measurement is based on simulated data generated for various Z' mass points (Table 8.1). All Monte Carlo (MC) samples were generated using PYTHIA with CTEQ6LI PDFs. The width of the generated Z' is 3% of the mass.

8.2.1 Muon selection

The nominal muon object selection includes an isolation requirement, which normally removes events where the signal lepton is found in a region of the calorimeter with large amounts of activity. Cutting on the amount of energy deposited in the calorimeter around the lepton is an example of one such requirement. Such a cut forms part of the object selection used in the top cross-section measurement described in Part 6.

However, as described a priori, boosted top events result in large collimated jets which include the products of the two top quarks. Thus the signal lepton can emerge within the cone of the reconstructed jet from the b-quark.

Note that the muon is not required to be isolated, instead the muon is tagged by the χ^2_{match} tagger. Selecting isolated muons would reduce significantly the number of muons available for tagging. Additionally, as explained a priori, events which exhibits stronger collimation are more likely to emerge from particles with higher masses. By requesting the muons be isolated, the ability to probe those higher mass events is diminished.

Another candidate to replace the traditional isolation selection is the so-called mini-isolation. This variable takes into account the strong collimation of the top products with increasing boost. Mini-isolation is defined as the sum of the measured transverse momenta of all tracks in a cone of size of size $\Delta R = k_T/p_T^\ell$ around the lepton, where

Table 8.2: Muon reconstruction selection used by Mini-Isolation and by Muon Tagging

| Mini-Isolation | Muon-Tagging |
|------------------------|------------------|
| MCP Cuts | |
| $p_T > 20 \text{ GeV}$ | |
| $ \eta < 2.5$ | |
| MUID | STACO |
| $z_0 < 3.0 \text{ mm}$ | Is Combined Muon |
| IsEM Tight | |

k_T is an adjustable scale and p_T^ℓ is the momentum of the lepton in question. This is known as the absolute mini-isolation. This study uses the relative mini-isolation where the absolute value is scaled by the momentum of the lepton (MI/p_T^ℓ).

In this analysis the performance of the χ_{match}^2 tagger is measured against mini-isolation using a $k_T = 10$ and a lepton is deemed isolated if the p_T in the MI cone is less than 5% that of the lepton. The Muon Tagger operates with the same selection as used in Part 6, the cuts are $z_0 < 3.0 \text{ mm}$, $d_0 < 3.0 \text{ mm}$ and finally $\chi_{\text{DoF}}^2 < 3.2$.

Thus two separate selections are applied, one for mini-isolation and one for SMT. Note that both methodologies have different muon reconstruction criteria, these are detailed in Table 8.2.

The performance of both methodologies are then compared by measuring their efficiency.

8.3 Efficiency definition

The efficiency measurement was designed to provide an accurate representation of the performance of the soft muon tagger and a valid comparison with mini-isolation. Additional sources of inefficiency such as muon reconstruction are separated out into an additional efficiency which is also quoted. See Figure 8.7 for a summary of the efficiency measurement.

Firstly, events where a W decays into a muon are selected, this becomes the pool of events from which the efficiency is measured. The selections then diverge and the two sets of reconstruction cuts described in Table 8.2 are applied independently. The efficiency of each sets of reconstruction cuts are measured as:

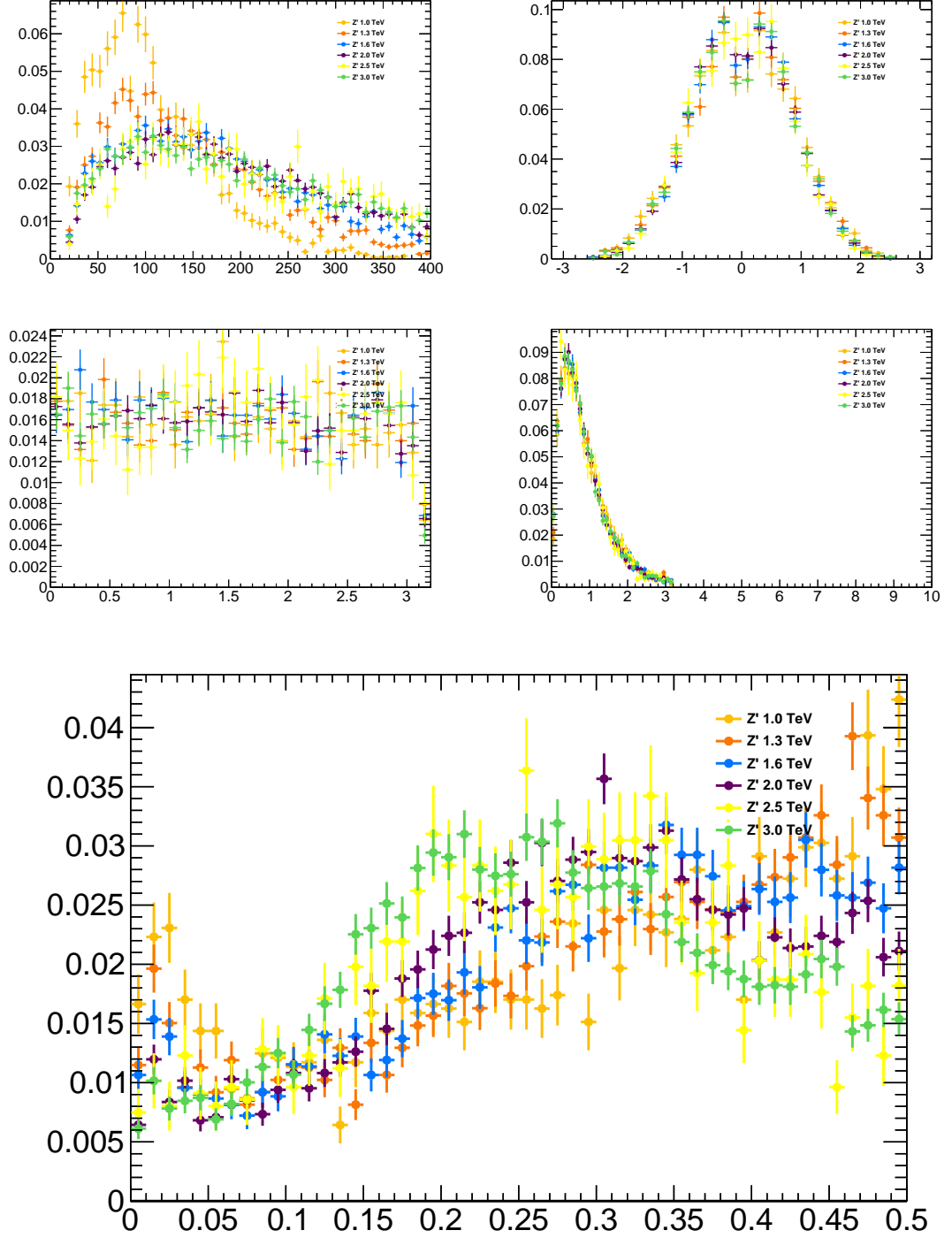


Figure 8.5: Control plots for muons which pass the χ^2_{match} tagger selection for all tested Z' mass points.

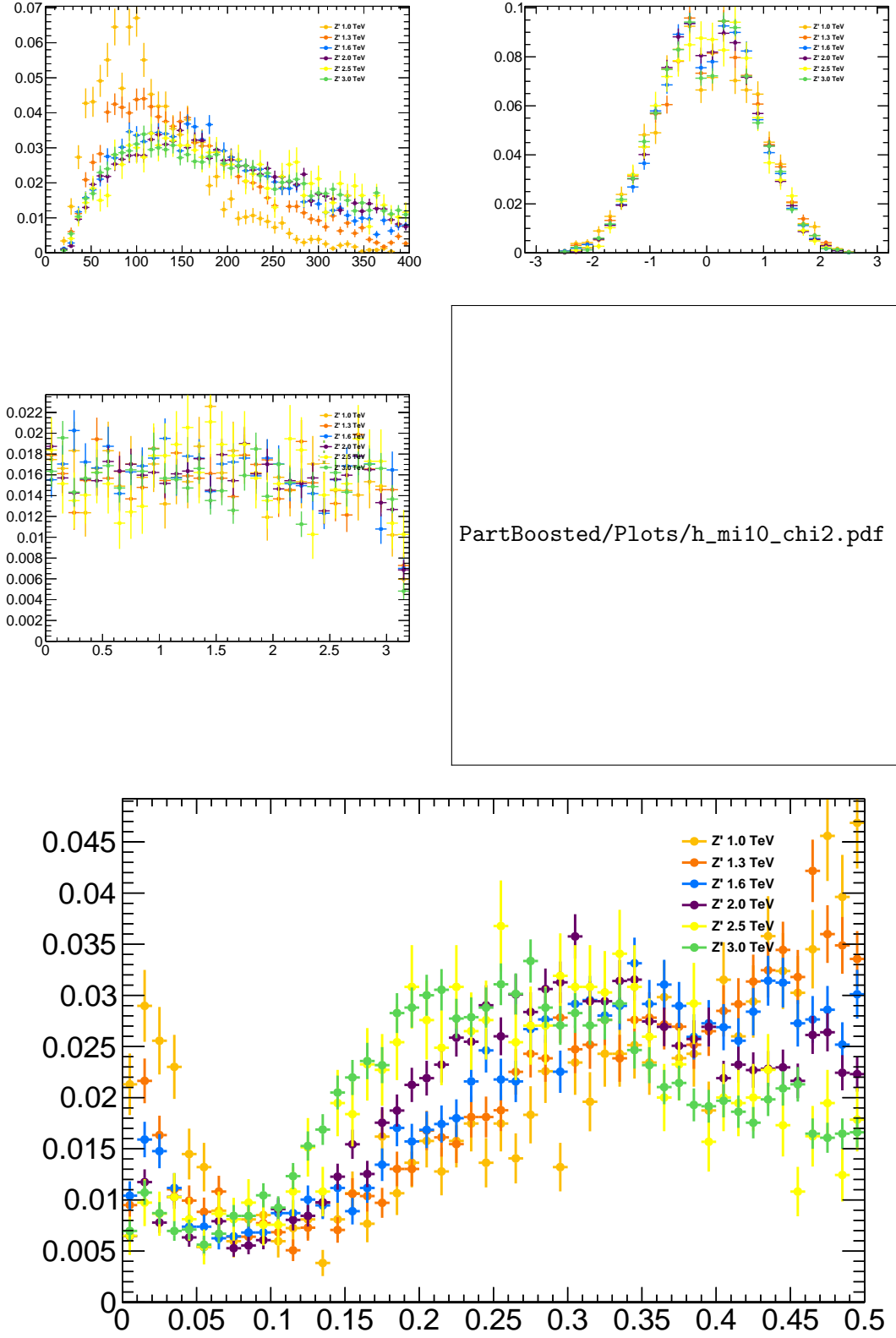


Figure 8.6: Control plots for muons which pass the mini-isolation selection for all tested Z' mass points.

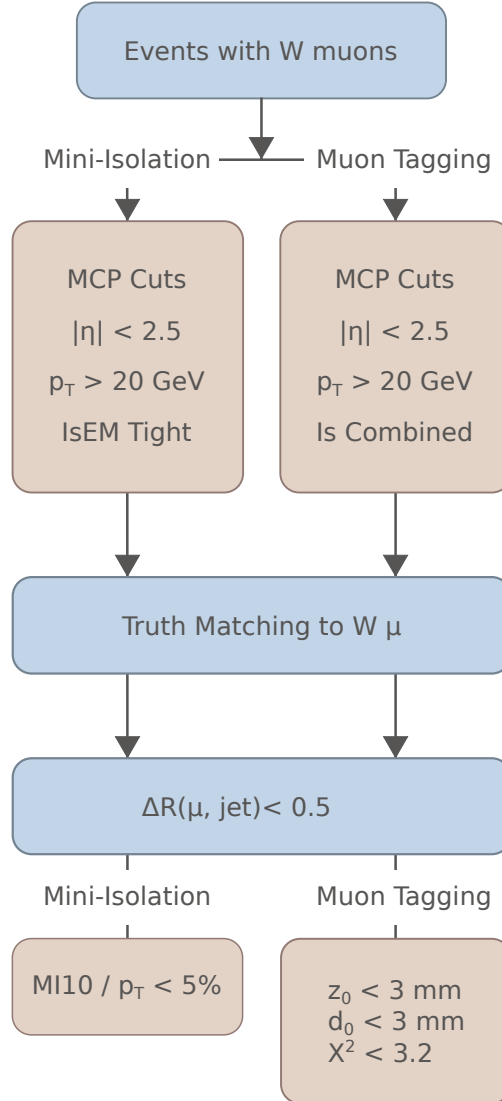


Figure 8.7: Structure of the efficiency measurement.

$$\epsilon_{\text{reco}} = \frac{\text{Muons which pass selection}}{\text{All reconstructed muons}}$$

These good reconstructed muons are then truth-matched to the truth μ from the W if the angular separate (ΔR) between them is less than 0.01. This has an efficiency associated with it, defined as:

$$\epsilon_{\text{match}} = \frac{\text{Muons matched to truth } W \text{ muon}}{\text{Muons which pass selection}}$$

Note that at each stage the denominator is the numerator of the previous efficiency. This allows for a combination of all the efficiencies to obtain an inclusive measure which can be used to approximate the number of W muons which would be selected from collision data assuming that the simulation describes the data well.

Next the muons are required to be within $\Delta R < 0.5$ from a jet. The Muon Tagger requires that jets be near a jet, in addition the impetus behind the analysis is to probe highly boosted events exploiting the capabilities of χ_{match}^2 tagging. This selection ensures that the muons available for χ_{match}^2 tagging are indeed close to a jet. This selection also has an efficiency associated with it defined as:

$$\epsilon_{\text{non-iso}} = \frac{\text{Muons with } \Delta R(\mu, \text{jet}) < 0.5}{\text{Muons matched to truth } W \text{ muon}}$$

The final step is the application of both the mini-isolation selection and the muon tagging selection discussed a priori. These selections are associated with the final and most interesting sets of efficiencies, defined as:

$$\epsilon_{\text{MT/MI10}} = \frac{\text{Muons which pass MT/MI10 selection}}{\text{Muons with } \Delta R(\mu, \text{jet}) < 0.5}$$

Please note that the denominator in every efficiency is a subset of the previous denominator. In other words each selection is applied in sequence and the efficiencies are calculated out of the remaining muons which passed the previous selection criteria.

Note that in the nominal analysis described in [3] muons which are within ΔR of 0.1 of the jet would be removed. The impetus behind the analysis is to exploit the χ_{match}^2 tagger to accept additional events where the signal muon emerges very close

to the jet axis, thus overlap removal is not part of the χ^2_{match} tagging selection. In order to provide an accurate performance comparison between the χ^2_{match} tagger and mini-isolation, the overlap removal is applied only for the mini-isolation selection at the end of the chain. The additional acceptance by the χ^2_{match} tagger is compared to the mini-isolation selection with overlap included:

$$\epsilon = \frac{\text{Muons that pass } \chi^2_{\text{match}} \text{ tagger} - \text{MI muons } \Delta R < 0.1}{\text{Total } W \mu}$$

8.4 Results

Mini-isolation is a very efficient method for selecting muons. Across the used mass range, the efficiency of selection remains above 80% and in fact increases with an increased Z' mass. When the Z' has a mass of 3 TeV the efficiency of selection with mini-isolation is 92.5%. In contrast the efficiency of the χ^2_{match} tagger is more consistent across the used mass range and higher than mini-isolation for a given mass. For a Z' with a mass of 3 TeV the measured efficiency of the χ^2_{match} tagger is 96.2%. When applying the overlap removal the efficiency of mini-isolation drops to 98%. As can be seen from Figure 8.8 the efficiency of mini-isolation dips for muons which are close to a jet. Note that this is below the threshold of the overlap removal.

8.4.1 Background

A preliminary examination of the amount of background was performed. This was done on the same sample of events but instead of selecting semileptonic events, the all-hadronic events are used as background. While these events do not perfectly mimic the true background, namely $b\bar{b}$, the lack of any real signal muons can provide a suitable preliminary substitute.

The lack of an isolation requirement is expected to result in a substantial increase in the amount of background selected. Additionally the semileptonic b -decays in $b\bar{b}$ would result in muons that the χ^2_{match} tagger will select. The analysis chain described in Section 8.3 is repeated on the same sample used a priori however the truth level selection of events with a W muon is reversed, thus at truth level both W bosons decay

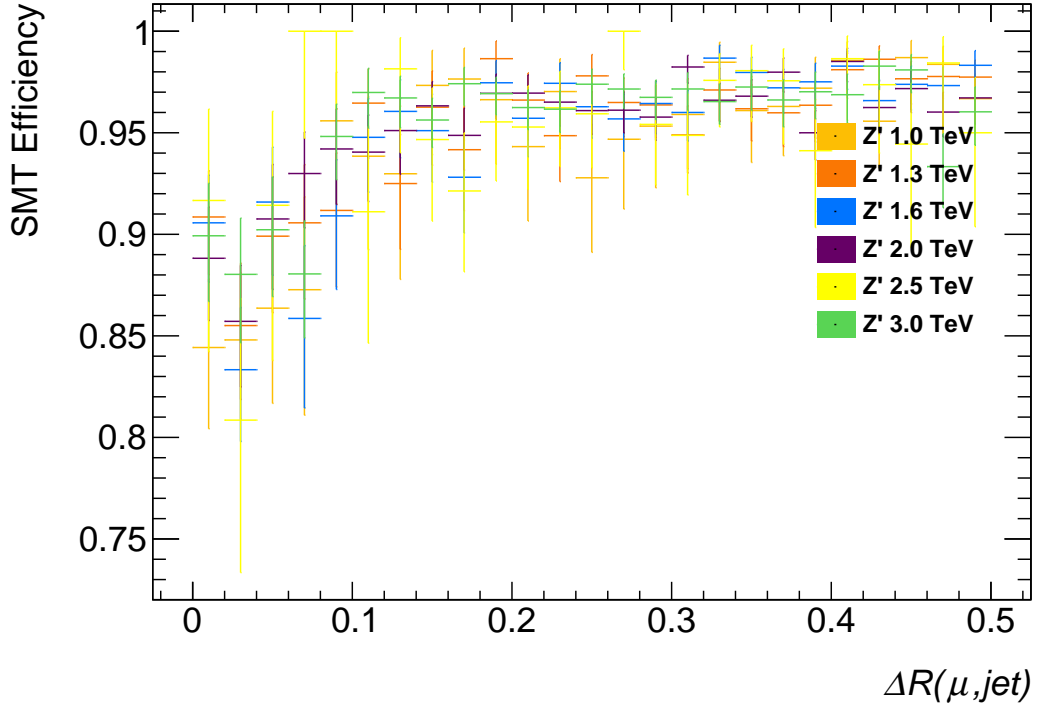
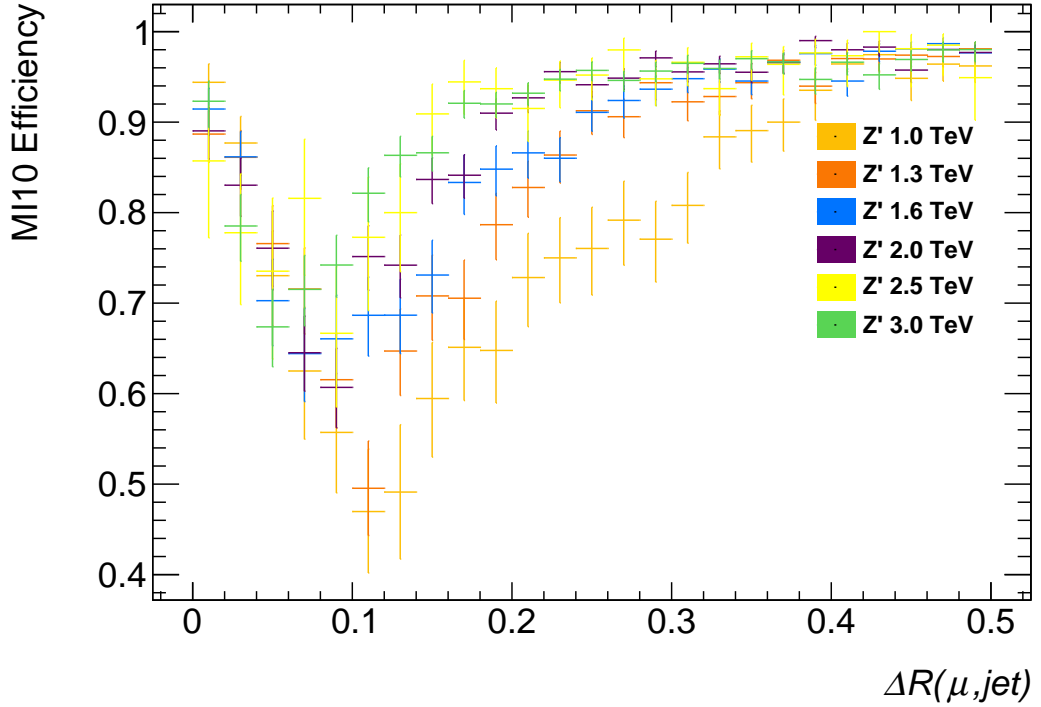
(a) χ^2_{match} muon tagger(b) Mini-isolation with $k_T = 10$

Figure 8.8: Efficiency of mini-isolation ($k_T = 10$) and χ^2_{match} muon tagger as a function of the angular separation between the reconstructed muon and the nearest reconstructed jet. Note the dip in the mini-isolation efficiency at low ΔR . In the nominal analysis an overlap removal between the jet and the muon is applied.

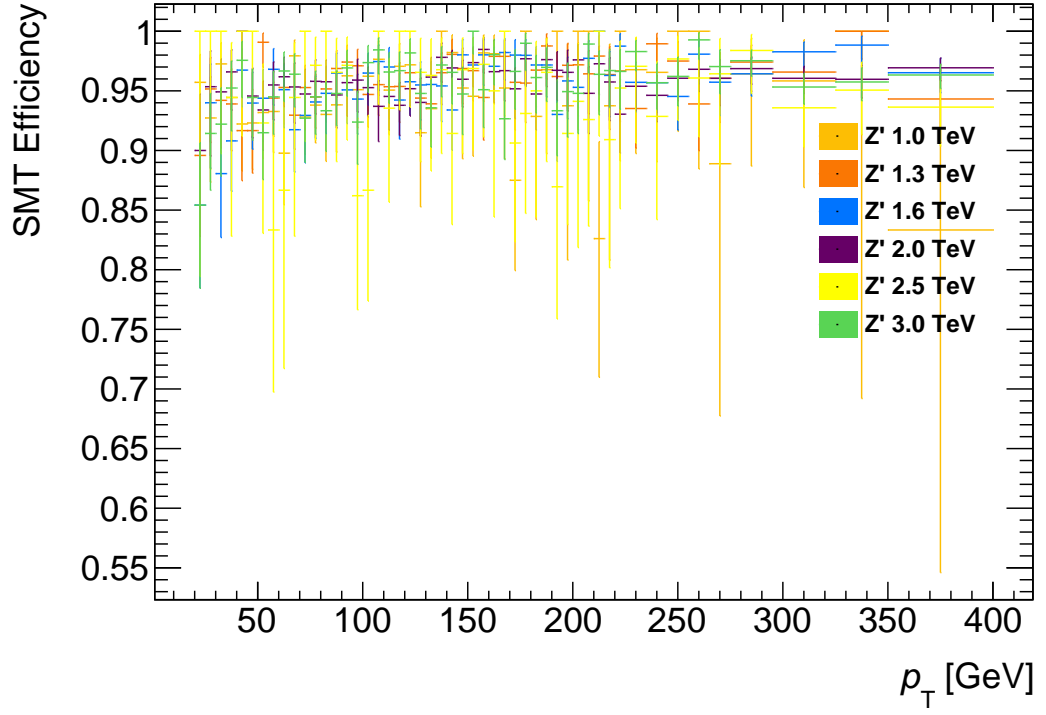
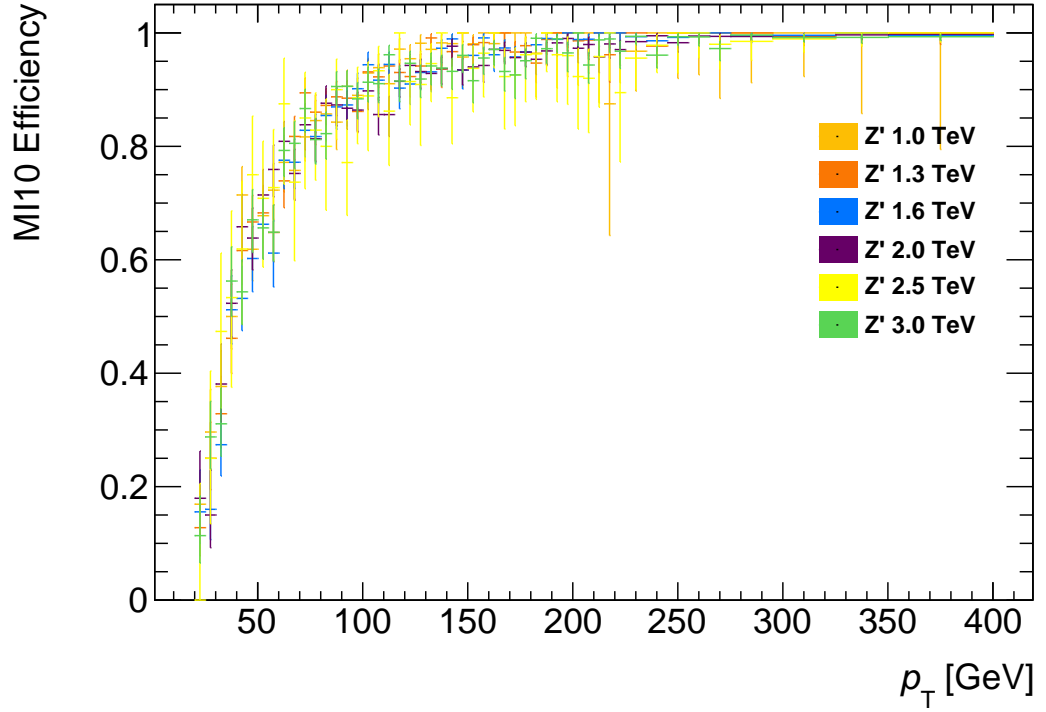
(a) χ^2_{match} muon tagger(b) Mini-isolation with $k_T = 10$ Figure 8.9: Efficiency of mini-isolation ($k_T = 10$) and χ^2_{match} muon tagger as a function of the transverse momentum of the muon.

Table 8.3: The efficiency measured in a selected background events.

hadronically.

The results of this selection are presented in Table 8.3.

Chapter 9

Conclusions

Bibliography

- [1] A search for $t\bar{t}$ resonances in the lepton plus jets final state with ATLAS using 14 fb^{-1} of pp collisions at $\sqrt{s} = 8\text{ TeV}$. Technical Report ATLAS-CONF-2013-052, CERN, Geneva, May 2013. Not published in the proceedings.
- [2] Search for $t\bar{t}$ resonances in semileptonic final state. Technical Report CMS-PAS-B2G-12-006, CERN, Geneva, 2013.
- [3] Georges Aad et al. Search for $t\bar{t}$ resonances in the lepton plus jets final state with ATLAS using 4.7 fb^{-1} of pp collisions at $\sqrt{s} = 7\text{ TeV}$. *Phys.Rev.*, D88(1):012004, 2013.
- [4] Serguei Chatrchyan et al. Search for anomalous $t\bar{t}$ production in the highly-boosted all-hadronic final state. *JHEP*, 1209:029, 2012.
- [5] Serguei Chatrchyan et al. Search for Z' resonances decaying to $t\bar{t}$ in dilepton+jets final states in pp collisions at $\sqrt{s} = 7\text{ TeV}$. *Phys.Rev.*, D87:072002, 2013.